High-Resolution Photoemission Study of Different NTCDA Monolayers on Ag(111): Bonding and Screening Influences on the Line Shapes†

Achim Schöll, Ying Zou, Thomas Schmidt, Rainer Fink,‡ and Eberhard Umbach*

Experimentelle Physik II, Universität Würzburg, Am Hubland, D-97074 Würzburg, Germany

Received: March 4, 2004; In Final Form: May 24, 2004

We present high-resolution C 1s and O 1s photoemission results of different NTCDA monolayer states adsorbed on a Ag(111) substrate (NTCDA = 1,4,5,8-naphthalene-tetracarboxylic acid dianhydride). The comparison of mono- and multilayer data clearly proves the chemisorptive character of the bonding of this planar aromatic molecule to the metal substrate. The rich fine structures of the monolayer spectra exhibit large differences for the three distinct monolayer states observed, leading to the conclusion of significant differences in their bonding. The fine structures are interpreted in detail on the basis of a thorough peak-fit analysis which allows a consistent assignment of the various photoemission main and satellite lines. As a result, the binding energies of the 1s levels of all C and O atoms and the relative intensities of the most significant satellite lines are extracted, the latter providing important information on the bonding and the dynamic screening process.

1. Introduction

In hybrid systems, the interfaces between different materials often play a decisive role for their functionality and properties. This is particularly true for systems consisting of organic and metallic components such as organic electronic devices (e.g., organic light emitting diodes (OLEDs), displays, field effect transistors (OFETs), and sensors). In such hybrids, the interaction between the molecules and the metallic substrates (or top contacts) determines the molecular orientation, structural order, film growth, interface dipoles, band offsets, band bending, etc., and hence the morphology and structure of the organic film, the charge carrier injection and transport, and even the (electro- or magneto-)optical properties. Thus, the detailed understanding of the organic/metal interface is of prime importance for various applications, especially if tailoring, optimization, or certain functions of organic devices are desired. Moreover, such a detailed understanding is also of fundamental interest in basic research, since the illumination of the adsorption behavior of large ($>\sim$200 amu) organic molecules on well-defined metallic substrates is a significant extension of the deep knowledge on small molecular adsorbates which were the target of numerous investigations[1] and the major issue of surface science for many years.

Because of the importance of this interface, numerous studies have been performed for various organic−metal combinations with particular emphasis on the bonding and the electronic structure, especially on the formation of interface dipoles. These interface dipoles had essentially been ignored ("Mott-Cabrera rule") when the gold rush on organic thin films and devices started in the early nineties. Moreover, there was the belief of many researchers that large organic molecules bond to the substrate essentially by van der Waals ("physisorptive") or electrostatic interaction, if they do not dissociate. Of course, such questions can be answered by using surface sensitive techniques, as done by several researchers. Most of these investigations, however, were performed on poorly defined interfaces (i.e., polycrystalline and/or dirty substrates, SiO_2, indium tin oxide, etc., with disordered or amorphous organic layers). Under these conditions broad spectroscopic features are observed, which are due to inhomogeneous broadening or averaging and hence hide the spectroscopic details which in principle could carry a wealth of information. Until now, only rather few investigations were performed on well-defined surfaces such as highly ordered monolayers of identical adsorbates on a well-prepared, clean, and ordered surface of a crystalline substrate.[9−15]

To get a deeper insight into the bonding of large organic molecules, we performed a model study on a well-characterized system, NTCDA on Ag(111), by means of high-resolution X-ray photoelectron spectroscopy (XPS) using highly monochromatic synchrotron radiation. We have chosen the heteroaromatic molecule NTCDA (1,4,5,8-naphthalene-tetracarboxylic acid dianhydride) since it shows at least three different adsorbate states in the monolayer regime on the (111)-oriented Ag single-crystal surface. These states were well characterized by various surface-sensitive techniques as outlined below. The aim of this study is to learn more details about the NTCDA/Ag interface, the different adsorbate states, and their bonding mechanisms, and to explore the potential of high-resolution X-ray photoelectron spectroscopy for such interface studies.

The previous experiments in our group can be subdivided into two groups, experiments on monolayers and on multilayers. Monolayer experiments using low energy electron diffraction (LEED) allowed us to distinguish two different long-range ordered superstructures at room temperature,[10] a densely packed superstructure at saturation coverage ($\theta = 1$), called the compressed monolayer (CM), and a less densely packed, the so-called relaxed monolayer (RM) that occurs for $\theta < 1$ (together with CM) and is exclusively observed for $\theta < 0.8$.[10,15] Recent spot profile analysis LEED (SPA-LEED)

† Part of the special issue "Gerhard Ertl Festschrift".

* To whom correspondence should be addressed. E-mail: umbach@physik.uni-wuerzburg.de.

‡ Present address: Physikalische Chemie II, Universität Erlangen, Egerlandstrasse 3, D-91058 Erlangen, Germany.

10.1021/jp049005z CCC: $27.50
Published on Web 07/14/2004

measurements[17] revealed that only the RM superstructure is commensurate to the substrate with the superstructure matrix

$$\begin{pmatrix} 4 & 0 \\ 3 & 6 \end{pmatrix}$$

whereas the compressed monolayer CM (which initially was believed to be commensurate, too) has a point-on-line superstructure with the matrix

$$\begin{pmatrix} 3.97 & 6.52 \\ -2.98 & 0.58 \end{pmatrix}$$

In this latter study, also a third, intermediate superstructure was found which is uniaxially incommensurate to the substrate. Since this third superstructure could not be prepared as pure adsorbate state, but only as mixture with the CM structure, it will be ignored in the present study. Scanning tunneling measurements[15] furthermore revealed that in the intermediate coverage range ($0.8 < \theta < 1$) ordered stripes with alternating RM and CM superstructures occur which can be reversibly broadened (RM) and narrowed (CM) upon partial thermal desorption, or narrowed (RM) and broadened (CM) upon readsorption of molecules. Very recently, a completely disordered fourth monolayer species was observed by SPA-LEED when the sample was cooled to about 150 K.[17] The spectroscopic signature of this disordered, low-temperature species (LT) is independent of coverage, i.e., independent of the initial superstructure from which the disordered phase is created upon cooling.

Near-edge X-ray absorption (NEXAFS) measurements were also performed using different polarization directions. From the strong polarization dependence, i.e., the linear dichroism, it was unambiguously derived that in all monolayers the molecules were "flat lying", i.e., that the molecular plane was oriented parallel with respect to the substrate surface.[11,16,18] In these NEXAFS studies, as well as in UV photoemission (UPS) and high-resolution electron energy loss spectroscopy (HREELS) measurements, it was observed that the LT monolayer phase, on one hand, and the CM or RM phases, on the other hand, can clearly be distinguished by their spectroscopic signatures, whereas the CM and RM phases look very similar.[18] Furthermore, it is noteworthy in context with the discussion below, which will particularly address the interfacial bonding of NTCDA on Ag(111), that the complete monolayer can be desorbed as intact molecules if the sample is heated to $T > 440$ K.[16] This finding as well as the spectroscopic signatures exclude any dissociation.

Multilayer experiments are performed using structural as well as electronic probes.[19−21] Although LEED experiments indicate that thin NTCDA films can be prepared with long range order under certain conditions,[16,18] NEXAFS experiments clearly show that at least three different layer morphologies with different molecular orientations with respect to the surface can be grown.[18,20,21] At low temperature (<200 K) and low deposition rates (<0.3 nm/min), a metastable layer of flat lying molecules can be established,[21] whereas around room temperature and for higher deposition rates (>1 nm/min), layers with either upright standing[21] or tilted molecules (or mixtures thereof) can be grown depending on the details of the preparation.[18] The electronic features of these multilayers are very similar in all spectroscopic data (also in XPS); however, only in high-resolution NEXAFS measurements a slight difference was found.[22] The NEXAFS results thus showed that the molecular orientation in multilayers can be "manipulated" by a proper selection of the preparation parameters.[21]

Finally, a strong influence of the substrate material and surface orientation on the bonding and structural order of NTCDA could be demonstrated for NTCDA monolayers on various Ag ((100), (110), (111)), Cu (100), and Ni(111) surfaces using LEED, UPS, and NEAXFS.[10,11]

In this work, we present a high-resolution X-ray photoemission study on three different NTCDA monolayer films on the Ag(111) surface. We intend to compare and to interpret consistently the spectroscopic finestructures of the three different monolayer species described above, denoted RM, CM, and LT, and of the multilayer. These different adsorbate states are interrelated by reversible structural phase transitions and characterized by flat-lying monolayer molecules directly attached to the substrate. The high quality of the present XPS data and a detailed peak fit analysis which consistently and simultaneously analyses all spectra enable us to determine the binding energies of all different carbon and oxygen atoms as well as the energies and intensities of several rather intense satellites. The latter are not only important for a correct qualitative interpretation and quantitative analysis but are also interesting because they reveal dynamic screening processes and their changes as a function of adsorbate state. Such satellites, which are often called shake-up satellites, have been investigated and classified for molecules in the gas phase[23−26] and various small adsorbates in detail.[27−32] Also for organic molecules, such satellites have been studied in the gas phase and in the condensed state by both experimental and theoretical methods. They allow further insight into the intramolecular and intermolecular response and into the response of the substrate to the creation of a core hole in the adsorbate upon photoionization. Strong differences of these satellites for the various atoms and for the different monolayer states are observed in this work which will be discussed qualitatively.

2. Experimental Section

The spectra were recorded at the U49/1-PGM undulator beamline at BESSY II. This soft X-ray beamline provides photon energies between 100 and 1500 eV with high spectral resolution and high photon flux. An energy resolving power of $E/\Delta E > 10\,500$ was experimentally derived at the N−K edge (at 401 eV) from the Gaussian contribution to the line width of the vibronic states which are resolved in the N 1s $\rightarrow \pi^*$ resonance in the NEXAFS spectrum of gaseous N_2 (photon flux: 3×10^{10} ph/s/100 mA). All C 1s and O 1s XPS spectra presented in this work were recorded with a photon energy of 335 and 700 eV and a photon line width of 26 and 88 meV, respectively.

The beamline has a spectroscopy endstation which consists of a two chamber ultrahigh vacuum system. It allows in situ surface cleaning and monolayer or film deposition in a preparation chamber (equipped with a sputter gun, LEED optics, and a Knudsen cell for evaporation of organic substances) and direct sample transfer to the analysis chamber equipped with a SCIENTA SES200 electron energy analyzer[37] for high quality photoemission experiments. This analyzer was operated with a constant pass energy of 40 eV corresponding to an analyzer energy resolution of $\Delta E = 80$ meV. The overall experimental resolution (analyzer plus beamline) can thus be calculated to 84 meV for the C 1s and 119 meV for the O 1s data. Analyzer and beamline were carefully energy-calibrated according to ref 38.

The NTCDA films were prepared under UHV conditions (base pressure below 2×10^{-10} mbar) by organic molecular beam deposition (OMBD) onto the clean and well-ordered

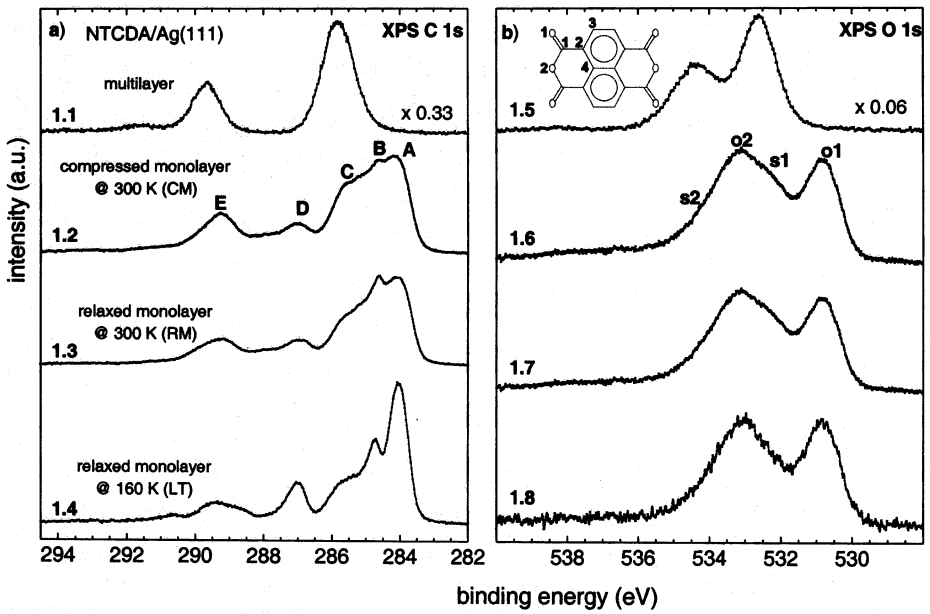

Figure 1. (a) C 1s and (b) O 1s XPS spectra of various NTCDA monolayers and a multilayer (∼20 ML) on Ag (111), recorded with a photon energy of 335 eV (C 1s) and 700 eV (O 1s), respectively. The spectra of the three different monolayer species represent a compressed monolayer (CM; spectra 1.2. and 1.6), a relaxed monolayer (RM; spectra 1.3 and 1.7), and a low temperature (LT) modification of the RM layer (spectra 1.4 and 1.8). For details of the preparation and the structure of the films see text. The multilayer spectra from ref 39 (spectra 1.1 and 1.5) are multiplied by a factor of 0.33 and 0.06, respectively, for better comparison. In Figure 1b, a scheme of the NTCDA molecule is displayed, and the chemically different oxygen (O1 and O2) and carbon atoms (C1 to C4) are labeled.

Ag(111) single-crystal surface. Prior to deposition, the Ag substrate was cleaned by repeated cycles of argon ion sputtering (ion energy 600 eV) and annealing at 800 K and checked before film deposition by XPS, LEED, and NEXAFS. No traces of impurities could be detected, and sharp LEED spots indicated a high structural order. The monolayers were prepared with a deposition rate of 0.5 ML (monolayer) per min onto the substrate at room temperature.

All samples were checked carefully for radiation damage during data acquisition. No sample degradation was observed on the time scale (∼1 h) of the experiments presented here. The XPS spectra were background-corrected by subtracting the sum of an exponential and a Shirley function, thus eliminating the influence of secondary and multiply scattered electrons.

3. Results and Discussion

3.1. Experimental Data. Figure 1 shows the C 1s (a) and O 1s (b) XPS spectra of condensed NTCDA multilayers (thickness ∼20 ML) compared to those of the three different monolayer states mentioned before. In Figure 1b, also the molecular structure formula of the NTCDA molecule is displayed, and the chemically different oxygen (O1 and O2) and carbon atoms (C1 − C4) are indicated.

The C 1s and O 1s multilayer spectra (1.1 and 1.5) were multiplied by a factor of 0.33 and 0.06, respectively, to allow for a better comparison with the monolayer data. A detailed analysis of the multilayer spectra in comparison with those of four other, similar molecules will be presented in ref 39. In the C 1s data (spectrum 1.1), the low binding energy (BE) peak belongs to the ring carbon atoms (C2 − C4), and the peak at 289.7 eV to the anhydride carbon C1. The small peak at 291.7 eV is assigned to a HOMO − LUMO shake-up satellite of the C1 peak. The O 1s data (spectrum 1.5) show two peaks that can be attributed to the O1 (532.6 eV) and the O2 oxygen atoms (534.4 eV). An O1 HOMO − LUMO shake-up satellite at 535.1 eV which belongs to the O1 peak is buried underneath the O2 peak.

For all monolayers, we observe very strong changes in the spectra as compared to the multilayers due to the interaction with the Ag(111) surface. These changes include BE shifts of more than 2 eV, which are significantly different for the various atoms, and drastic shifts of spectral weight from the main peaks to the satellites. As mentioned above, these changes are not due to dissociation which can unambiguously be derived from the fact that the NTCDA molecules can be completely desorbed by heating and that the phase transitions between the different monolayer states are completely reversible. Therefore, we must in each case unambiguously conclude a distinct chemisorptive character of the adsorbate bonding to the substrate. This finding is consistent with all other spectroscopic data from, e.g., UPS,[40] NEXAFS,[11] and HREELS.[41]

Next, we analyze the spectra in more detail. In the C 1s spectra of Figure 1a, a strong shift of the ring carbon peaks toward lower binding energy from multilayer to monolayer is observed. This shift (about 2 eV, from 286 to 284 eV, for the peak maximum) is most likely due to the additional screening of the core hole in the molecule by dynamic charge transfer from the metal substrate to the molecule. We derive this interpretation from the fact that the charge state of the molecule remains nearly constant in the monolayer (nearly no work function change is observed[40]) and from the experience gained from many adsorbate systems which show such large BE shifts together with nearly no work function change only if charge-transfer screening occurs.[27] In a simple physical picture, charge-transfer screening occurs when a core hole in an adsorbate is created by photoionization and the adsorbate is well coupled to the substrate. In this case, a previously unoccupied orbital which is pulled down in energy below the metal Fermi level by the additional core hole potential in the molecule can become filled by an electron that is quickly transferred from the metal into this molecular orbital. This leads to a neutralization of the molecule and hence to a very effective reduction of the BE of the ionized level. Of course, this screening process always occurs, no matter how strongly the

molecule is coupled to the substrate. However, only for strongly coupled systems, the transfer process is fast enough to contribute to a BE reduction on the time scale of the photoionization process. Thus, large BE shifts (>1.5 eV) between monolayer and multilayer are usually due to charge transfer screening, especially if all molecular core levels are similarly affected, while smaller BE shifts (<1.5 eV) could also be due to screening by polarization of the neighborhood (including image potential screening).

The ring carbon peak of the multilayer splits into several distinct peaks for all monolayers, namely two well resolved peaks, denoted (A) at 284 eV and (B) at 285 eV, that can be attributed to different ring carbon atoms, and a broad shoulder (C) at the high BE side. The peak (D) at 287 eV can be attributed to the anhydride carbon (for the assignment, see below) and is shifted by nearly 3 eV with respect to the multilayer. This relatively large shift indicates that the carbon atom of the functional group, which is least screened in the molecule due to the electronegativity of the oxygen atoms in the anhydride group, profits most from the additional screening channel in the interfacial state. At higher binding energies with respect to the main peaks, several strong satellite peaks, e.g. peak E at 289 eV, are resolved, which will be analyzed and assigned later. It will also be shown that structure E is not the remnant of the anhydride peak at 289.5 eV in the multilayer.

Interestingly, the spectra of all monolayer states basically show the same spectral features at similar energetic positions but with drastically different intensities. If we compare the RM with the CM species, the about 20% lower coverage mainly leads to a lower intensity of the shoulder (C) at 286 eV and of the satellite peak (E) at 289.5 eV. It is emphasized at this point that the detection of such differences is only possible because of the high quality (resolution and signal-to-noise ratio) of these data and that a distinction of three monolayer states is very remarkable by itself. Although slightly different geometrical structures could be distinguished by SPA-LEED and STM for the CM and RM states, respectively, it could be argued that such large, flat-lying molecules would "average" over several Ag atoms and hence would not show specific differences in bonding due to different adsorption sites when slightly shifted on the surface. The present data clearly prove that the electronic structure of large organic adsorbates depends very much on the specific adsorption site or, in other words, that subtle differences occur in the bonding which depend on the specific structural details. This remarkable observation is consistent with the conclusion of chemisorptive bonding.

If the RM film is cooled to 160 K, resulting in the LT spectra, the relative intensities in the C 1s data change drastically. Again, the 286 eV shoulder (C) and the 289.5 eV peak (E) decrease, but simultaneously, the photoemission lines (A) at 284 eV and (D) at 287 eV strongly increase. These striking differences in the core level spectra indicate strong differences in the bonding mechanism to the substrate for the monolayers at different substrate temperatures (RM − LT).

The O 1s data (Figure 1b) of the NTCDA monolayers are dominated by two peaks, which can be attributed to the two oxygen atoms in different bonding situations in the anhydride group, in analogy to the multilayer. As discussed in context with the C 1s data, the monolayer lines are also shifted toward lower binding energies. However, within the functional group, the screening effect on the oxygen core levels is smaller as compared to the anhydride carbon, indicated by the smaller energy shift of 2 and 1.5 eV for the O1 (o1 line) and O2 oxygen atoms (o2 line), respectively.

For all monolayers, the intensity ratio between the O1 and the O2 peak is far from the stoichiometric value of 2:1. This is easily explained by an intense satellite of the O1 peak that contributes to the intensity of the peak at 533 eV. This satellite is responsible for the shoulder (s1) at 532.5 eV, which is clearly visible in the CM and RM data (spectra 1.6 and 1.7, respectively). The shape of the O2 peak at the higher BE side indicates, that at least one further satellite (s2) around 534 eV has to be taken into account. We emphasize at this point that the usual simple assignment of each XPS peak to one chemical state thus neglecting the occurrence of satellites would lead to wrong chemical conclusions in the present case. Since in the monolayer data the peak at 533 eV is much more intense than that at 531 eV (which drastically deviates from the stoichiometric ratio of 1:2), one might be mislead and conclude a chemical reaction different from simple chemisorption. The present observation thus stresses the importance of taking satellite features into account, especially for the interface.

The differences in the O 1s data between the monolayers are in complete analogy to what we observed for the C 1s spectra. The energetic positions of the spectral features for the different monolayer states are almost unchanged, whereas a decrease of the intensity of the satellite peak (s1) at 532.5 eV from CM to RM and from RM to LT mainly accounts for the changes in the O 1s spectra of the different monolayer films.

3.2. Peak Fit Analysis. To further analyze the various spectroscopic features, i.e., to distinguish and assign the main lines and satellite structures in detail and to define their energetic positions, a detailed least-squares peak fit analysis was performed for the C 1s and O 1s spectra of Figure 1.

3.2.1. O 1s Spectra. The smaller number of spectral features that originate from only two chemically different oxygen species makes the O 1s data easier to interpret. Thus, we start with these. Spectrum 2.1 in Figure 2 shows the fit result of the multilayer O 1s spectrum (from ref 39). The peaks at 532.6 and 534.2 eV are attributed to the main photoemission lines of the O1 and O2 atoms. At 535.2 eV, an intense HOMO−LUMO shake-up satellite of the O1 peak is visible. An additional Gaussian function was applied to account for the background at about 538 eV, which is due to additional shake-up losses of both photoemission lines.

A minimum number of six peaks is needed to satisfyingly reproduce the monolayer O 1s spectra, as can be directly concluded from the experimental data. These are the O1 photoemission line at 530.8 eV (o1), the O1 satellite (s1), that due to intensity/stoichiometry reasons has to be attributed to the intense shoulder at 532.4 eV, the O2 photoemission line at 533 eV (o2), a satellite peak at 534 eV (s2), that for stoichiometric reasons has to be attributed to the O2 peak, plus two more peaks between 535 eV (s3) and 538 eV (bg), that generate the line shape and background of the spectra at higher binding energies.

Of course, various constraints have been used to reduce the number of free parameters in the fit function. For the main lines, Voigt profiles were used with a constant Lorentzian line width of 0.1 eV and an equal (= fit result) Gaussian line widths. All satellite peaks are represented by Gaussian functions. [Values of 0.1 eV for the lifetime broadening of the O 1s and 0.08 meV for that of the C 1s core hole were determined from the NEXAFS data of NTCDA and the similar molecules ANQ and BPDCA.[40] No indications for a different lifetime for the 1s states in the NTCDA monolayers were found in this work and in previous XPS experiments on NTCDA and similar molecules.[39]] Stoichiometric boundary conditions are that the intensity ratio

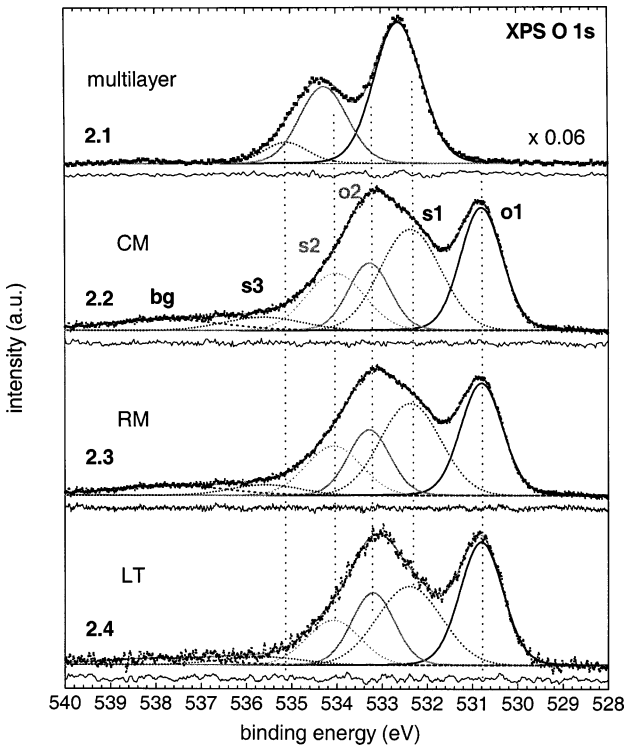

Figure 2. Results of the peak fit analysis of the O 1s spectra of the NTCDA compressed monolayer (CM, spectrum 2.2), relaxed monolayer (RM, spectrum 2.3), and low-temperature monolayer (LT, spectrum 2.4). The multilayer fit (spectrum 2.1) from ref 39 is plotted for comparison. For the main peaks o1 and o2, Voigt functions with a fixed Lorentzian width of 0.1 eV and Gaussian width which is equal for all spectra were used. The satellites s1, s2, and s3 as well as the background structure (bg) are accounted for by Gaussian peaks. The intensities are constrained by the stoichiometry of the atoms in NTCDA to 2:1. The residua (= difference between experimental spectrum and fit) are plotted below the spectra.

of the O1 and O2 main lines plus corresponding satellites has to be equal to 2:1, i.e.

$$\left(\mathrm{o1} + \mathrm{s1} + \mathrm{s3} + \frac{2}{3}\mathrm{bg}\right):\left(\mathrm{o2} + \mathrm{s2} + \frac{1}{3}\mathrm{bg}\right) = 2$$

Note, that the satellite s3 can be attributed to O1, as will later become clear. The area of the background Gaussian peak (bg) is included in the intensity ratio of O1 and O2 with a fraction of 2:1 since its origin is not unambiguously clear. However, from shake-up calculations[36] it is known that several weak satellites from both oxygen atoms arise in this energy range.

In Figure 2, the result of a peak fit analysis of the monolayer O 1s data using these constraints is displayed. The corresponding residua (i.e., measured data minus fit result; plotted underneath each spectrum) show the excellent quality of the fits. The energy positions, intensities, and line widths of the fitted peaks are summarized in Table 1 together with the χ^2 values (defined as $\chi^2 = \sum_n (I_{\mathrm{exp}} - I_{\mathrm{fit}})^2 / I_{\mathrm{exp}}$) of the corresponding optimal fit which are a measure of the fit quality. The dotted guidelines in Figure 2 indicate that between the different monolayer structures only minor changes of the energy positions of the spectral features occur. Note that the similarities of the peak energies of the different adsorbate states are an indicator for both the correctness of the fit result, since the peak energies were optimized independently in the various fits, and the similarity of the chemical state.

The chemisorption process involves the hybridization of the molecular π system with metal states. The resulting hybrid orbitals differ in character; they may have more metal or more adsorbate character. The latter can more effectively screen the adsorbate core hole, since they have a larger electron density on the molecule, resulting in a lower BE of the observed photoemission line. Thus, we can assume that the same orbitals are involved in the screening process for all monolayer modifications, resulting in essentially the same binding energies of the spectral features.

TABLE 1: Results of the Least-Square Peak Fit Analysis of the NTCDA O 1s Monolayer Spectra from Figure 2[a]

	CM			RM			LT		
	E_B (eV)	A	Γ_G (eV)	E_B (eV)	A	Γ_G (eV)	E_B (eV)	A	Γ_G (eV)
o1	530.80	0.28	1.03	530.79	0.25	1.04	530.80	0.28	1.06
o2	533.29	0.15	1.03	533.29	0.15	1.04	533.20	0.17	1.06
s1	532.37	0.32	1.59	532.37	0.29	1.58	532.40	0.27	1.69
s2	534.03	0.17	1.52	534.07	0.14	1.45	534.08	0.12	1.40
s3	535.62	0.05	2.04	535.57	0.04	1.82	535.66	0.03	2.15
Bg	537.84	0.07	3.01	537.71	0.06	3.01	537.96	0.04	3.01
χ^2	1.23×10^{-5}			1.23×10^{-5}			1.92×10^{-5}		

[a] The parameters are the binding energy E_B, the peak area A, the Gaussian width Γ_G of the fitted peaks, and the fit quality χ^2 defined in the text. For a detailed peak assignment, see the text.

Very intense satellites such as s1 and s2 are typical for photoemission spectra of weakly chemisorbed molecules and are well understood, e.g., for CO or N_2 on metal substrates.[27,29,30,42] Different theoretical approaches have been used to explain these features, e.g., by Bagus et al.,[43−47] by Messmer et al.,[48] and by Schönhammer and Gunnarsson.[49−51] It is commonly agreed that the charge transfer from the substrate that follows the core excitation to screen the core hole leads to different lines in the photoemission spectra. The line at lowest binding energy belongs to the well or fully screened core state (sometimes also referred to as "shake-down" satellite) as described above, whereas the lines at higher BE can be attributed to unscreened or poorly screened final states. The latter can be observed with very high intensity if the photoemission process and the charge transfer from the substrate occur on a similar,[27,51] which is the case for weak chemisorption.

In the present case, the binding energies of the poorly screened final states (i.e., the main satellites) are very similar to those of the main lines of the multilayer peaks, since in both cases only *intra*molecular screening processes are important. This is consistent with the description of the screening process and the interpretation given above. In this paper, we refer to the well or fully screened lines at lowest BE as main lines, since usually these lines are most intense, which is not always the case as shown here.

The assignment of s1 and s2 to poorly screened O 1s final states suggests the interpretation of s3 as shake-up satellite of the poorly screened O1s state (s1), in analogy to the multilayer spectra. This was anticipated in the intensity constraints for the fit analysis of the O 1s data, but even if this tentative assignment was incorrect, the final result would hardly be changed.

It is very interesting that the relative intensities of main and satellite peaks are rather different for the different monolayer states. This is demonstrated by Figure 3, in which the intensity ratios of the satellites (s1 + s3 and s2, respectively) and their corresponding main lines (o1 and o2, respectively) are plotted for the three different monolayer preparations. The satellites are more intense than the main lines for the CM structure, but their relative intensities decrease for the RM structure. For the LT layer, the satellite intensities are further decreased; they are about equal to the main line for O1 and smaller than the main line for O2.

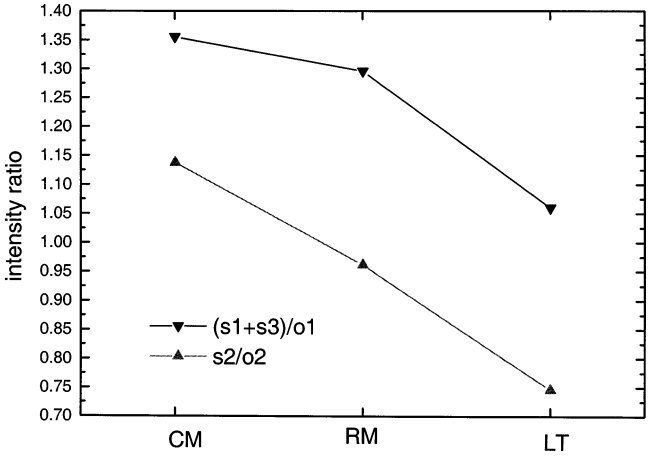

Figure 3. Intensity ratios of the satellite and main lines of the two different oxygen atoms O1 and O2, (s1 + s3)/o1 and s2/o2, respectively, for the three different monolayer species CM, RM, and LT.

The changes of the satellite intensities can easily be understood as changes of the probability of charge-transfer screening from the Ag substrate. That this probability is reduced is the result of subtle changes of the interface coupling. The probability that screening charge is transferred from the substrate to the NTCDA molecule upon photoionization is apparently highest for the LT adsorbate, resulting in a relatively small intensity of the poorly screened compared to the well-screened final state. The finding of Figure 3 implies that the adsorbate−substrate coupling slightly increases from the CM over the RM to the LT adsorbate species which is consistent with all other experimental findings and with the intuition that a compressed adsorbate structure consists of less well bound molecules than a relaxed structure in which the molecules can take the optimum adsorption sites. It is interesting to note that in the LT monolayer the molecules are apparently even more strongly bound as compared to the room temperature monolayers which is probably due to a less activated position of the LT molecules in the bonding potential and/or to a different potential curve because of rather different thermal expansion coefficients for substrate and molecular layer, respectively. In addition, we speculate that the monolayer molecules are slightly distorted upon chemisorption which certainly changes as a function of the adsorption site and would also lead to different potential curves.

3.2.2. C 1s Spectra. A complete analysis of the more complicated C 1s spectra is not as easy and straightforward as for the O 1s spectra. Four distinguishable carbon atoms (labeled C1−C4 in the inset of Figure 1b) causing different C 1s main lines and satellites have to be considered, leading to the rich spectra 1.2−1.4 with various peaks and shoulders as presented in Figure 1a. We will try in the following to understand and assign the most prominent features in the C 1s data by a comparison of the different monolayer spectra and the preinformation from the analysis of the O 1s data.

We start with the LT monolayer (spectrum 4.4 in Figure 4), which shows the best resolved lines. If we integrate all peaks in spectrum 1.4 on the right (A1) or left side (A2) of the minimum at 286.5 eV and calculate the intensity ratio A1/A2, we find 2.47, which is very close to the stoichiometric ratio of 2.5 between naphthalene ring (10) and functional group carbon atoms (4). Thus, the assumption appears obviously justified that the intensity region between 283 and 286.5 eV can be attributed to the ring carbon atoms C2−C4, including their main and satellite lines, whereas all features above 286.5 eV belong to the anhydride atoms (C1). The very small deviation (∼1%) from

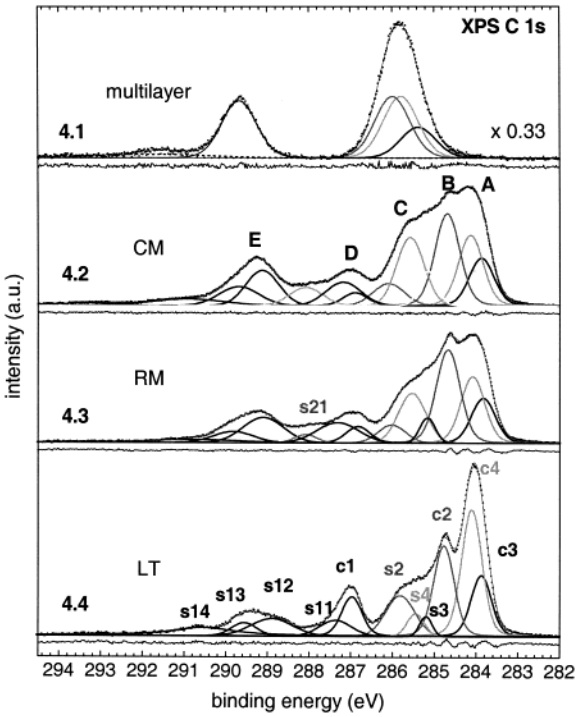

Figure 4. Results of the peak fit analysis of the C 1s spectra of the NTCDA compressed monolayer (CM, spectrum 4.2), relaxed monolayer (RM, spectrum 4.3), and low-temperature monolayer (LT, spectrum 4.4) in comparison with the multilayer fit (spectrum 4.1) from ref 39. For the main lines (c1−c4), Voigt functions with a fixed Lorentzian width of 0.08 eV and identical Gaussian widths were used. All satellite lines (s11−s14, s21, and s2−s4) are represented by Gaussian peaks. See text for detailed information about the constraints used. The residua are plotted below the spectra.

the stoichiometric ratio is within the error bar; it could be due to additional weak satellites of the naphthalene carbon atoms that are buried underneath the anhydride peaks or to an improper consideration of the background. Such influences are not important and do not change the main results and hence are omitted in the fit analysis. We further assume the same line shape for all main lines, since first, previous XPS and NEXAFS[22] experiments on NTCDA and similar molecules showed the same lifetime broadening for the different carbon atoms, and second, there is no obvious reason for differences in the Gaussian line widths, since the experimental resolution and inhomogeneous broadening should be equal.

Thus, for the naphthalene part, the peaks (A) at 284 eV and (B) at 285 eV have to be attributed to the main lines from the atoms C2−C4, the broad shoulder (C) at 286 eV to their satellites. This assignment arises from the quantitative comparison of the spectra from the three monolayer species. In the anhydride part of the spectrum, we identify the anhydride C1 main line at 287 eV which is accompanied by several anhydride satellites at higher BE.

As mentioned earlier, a comparison of the C 1s monolayer spectra clearly shows the strong decrease of the satellite peaks C and E from CM to RM and especially from RM to LT. This is in complete analogy to the analysis of the satellites in the O 1s spectra. Since the satellites C and E also coincide energetically very well with the multilayer ring and anhydride carbon lines at 286 and 289 eV, respectively, their assignment as poorly screened C 1s states of the ring and anhydride carbon atoms is very likely.

With these preconditions, a peak fit analysis of the LT spectrum can be performed. The result is displayed in Figure

TABLE 2: Results of the Least-Square Peak Fit Analysis of the NTCDA C 1s Monolayer Spectra from Figure 4[a]

	CM			RM			LT		
	E_B (eV)	A	Γ_G (eV)	E_B (eV)	A	Γ_G (eV)	E_B (eV)	A	Γ_G (eV)
c1	286.89	0.44	0.64	286.83	0.53	0.62	286.97	1.11	0.52
c2	284.69	3.11	0.64	284.67	3.03	0.62	284.77	2.56	0.52
c3	283.87	1.60	0.64	283.83	1.45	0.62	283.88	1.71	0.52
c4	284.13	2.38	0.64	284.08	2.15	0.62	284.11	3.58	0.52
S11	287.18	1.07	0.99	287.32	1.08	1.18	287.37	0.63	0.88
S12	289.13	1.48	0.92	289.11	1.32	1.15	288.90	0.92	1.16
S13	289.69	0.97	1.12	289.83	0.58	1.13	289.56	0.42	0.70
S14	290.94	0.63	2.06	290.78	0.38	2.62	290.56	0.98	1.77
s2	286.10	0.90	0.89	286.02	0.63	0.77	285.81	1.51	0.81
S21	288.08	0.78	0.94	288.09	0.24	0.63			
s3	285.15	0.79	0.50	285.16	0.50	0.43	285.20	0.32	0.35
s4	285.57	2.41	0.77	285.53	1.74	0.77	285.44	0.49	0.47
χ^2	7.65×10^{-4}			9.19×10^{-4}			1.84×10^{-3}		

[a] The parameters are the binding energy E_B, the peak area A, the Gaussian width Γ_G of the fitted peaks, and the fit quality χ^2. For a detailed peak assignment, see the text.

4, spectrum 4.4. The fit parameters were constrained as follows: for the main lines (c1−c4), Voigt profiles were utilized with a constant Lorentzian line width of 80 meV and an equal (resulting from the fits) Gaussian width. For all satellite peaks, Gaussian functions with variable widths were used since satellites are usually broader and have different line widths. For each ring carbon, one satellite was allowed (s2−s4), and for the anhydride carbon, four satellites had to be employed (s11−s14) in order to describe the observed features sufficiently well (see Figure 4). The ratio of the peak areas was constrained according to the NTCDA stoichiometry

$$(c1 + \text{satellites}):(c2 + s2):(c3 + s3):(c4 + s4) = 4:4:2:4$$

As start values, the satellite peaks s2−s4 were set in the same relative energetic order as the main lines c2−c4. A rather good fit result is obtained with these assumptions, as can be derived from the residuum plotted below spectrum 4.4.

All parameters resulting from this peak fit analysis and the analyses of the other C 1s spectra are summarized in Table 2. We see, that the photoemission lines c3 and c4 contribute to peak A, whereas peak B is generated by c2. The main contribution to shoulder C is satellite s2, which represents the poorly screened C 1s core hole final state of the carbon atom C2 while the carbon atoms C3 and C4 have much weaker satellites. In the anhydride part, peak D is mainly due to the c1 line, as mentioned. Satellite s12 can be attributed to the C1 poorly screened final state and satellite (s14 to an additional shake-up satellite, as in the multilayer data. Satellites s11 and s13 are most likely also due to shake-up losses of the c1 line. Note, however, that a distinction between "shake-up" peaks and "poorly screened final states" is artificial since both belong to the same type of final state, namely an excited ionic state, and could be described in a similar way by a theoretical approach.[33−36,43−48]

If the same fit function is applied to the RM spectrum 4.3, the most important changes between the two structures become very clear. The fit result is also displayed in Figure 4 (spectrum 4.3). The c1 and c3 lines are strongly reduced, whereas the respective satellites s12, s3, and s4 gain much intensity. Only, the c2 line is slightly increased while the s2 satellite is decreased. The same trend is followed if we compare the fit of the RM data (spectrum 4.3) with the fit of the CM data (spectrum 4.2).

The strong changes in the relative intensities of the signals from well and poorly screened core states, especially between the LT and RM structures, also indicate local differences in the charge-transfer screening of the core hole, as in the case of the O 1s data. However, whereas the C3 and C4 core holes appear to be better screened for the LT layer, the charge-transfer screening of the C2 and C1 holes seems to be less effective. For the CM layers, the C1 and C3 screening is even worse, whereas the C2 hole is now screened more effectively.

These very local changes of the charge-transfer probability of the ionization process for different core holes within the same molecule are most likely due to differences in the spatial distribution of the molecular orbitals, especially of the frontier orbitals which participate in the adsorbate−substrate bonding. Interestingly, the intensity ratio A1/A2 is decreased significantly for the RM (2.19) and CM (1.95) data, indicating that satellites from the ring carbon atoms now contribute more to the anhydride side of the spectra. To take this observation into account, a satellite peak (s21) had to be included in the fit, which can be interpreted as representative for shake-up satellites of naphthalene carbon atoms. Since SDCI calculations on the similar molecules PTCDA, NDCA, and PTCDI show the strongest shake-up intensity in the aromatic part for the C2 carbon atoms, we assign this peak to a C2 shake-up satellite s21. The intensity of satellite s21 was also included in the fit constraints.

4. Concluding Remarks

High-resolution C 1s and O 1s XPS spectra of NTCDA monolayers on the Ag(111) surface demonstrate a rich, well-resolved fine structure which carries a wealth of information. The finestructures are very different for the three distinct monolayer adsorbate states which are discussed in the present study and which are interrelated by reversible structural phase transitions. Thus, one main finding of the present study is the potential of high-resolution XPS to distinguish between slightly different adsorbate species even in the case of large organic molecules which, due to their much larger size as compared to the substrate unit cell, occupy very similar adsorption sites independent of the superstructure.

If the monolayer spectra are compared to those of weakly interacting NTCDA molecules in multilayers, we see strong differences that clearly demonstrate the chemisorptive bonding of NTCDA on the Ag(111) surface, the second main finding. The additional screening by charge transfer from the substrate shifts the main photoemission lines of the monolayer toward lower binding energy by 1.5−3 eV thus leading to their assignment as well-screened core hole final states. The high energy resolution allows us to distinguish the main lines and satellites of the various carbon and oxygen atoms in different bonding situations. A careful peak fit analysis enables us to assign the various spectral features in the XPS spectra and to derive binding energies for the chemically different oxygen and carbon atoms. The strongest satellite lines are attributed to poorly screened core final states, which occur especially for weakly chemisorbed adsorbates by an incomplete charge-transfer screening process on the time scale of the photoemission process. The demonstration that such satellites may be larger than the main lines which was until now only shown for small adsorbates in favorable cases (i.e., for weak chemisorption) is the third main finding of this work.

Finally, as the fourth main finding, our analysis yields very significant differences between the satellites in the three different adsorbate states. This result points toward subtle differences in the adsorbate−substrate coupling for the different NTCDA monolayer species. The trend of satellite intensities actually

suggests that the bonding strength increases from the compressed via the relaxed to the low-temperature monolayer, an interpretation that is in agreement with intuition and other experimental observations, none of which is as clear as the present result. The detailed analysis furthermore indicates local differences of the charge-transfer screening for the various atoms within the molecule.

We note that the present results should be sufficiently detailed to encourage sophisticated calculations to elucidate the details of the chemical bond of such adsorbates. These should include the dependence on the particular adsorption site, the spatial distribution, and the energetic positions of the molecule−metal hybrid orbitals, which participate in the adsorbate−substrate bonding, and their reaction upon creation of a core hole.

We further note that diffraction effects most probably do not influence our results. First, we did not observe any changes of the line shapes for varying emission angle or incident photon energy. Second, such effects are not expected because the molecules in the incommensurate CM or disordered LT layer have no fixed lateral position with respect to the substrate atoms, and even for the various O and C atoms of the two molecules per unit cell of the RM layer an averaging of backscattering from the Ag substrate atoms due to their very different relative positions must occur. We emphasize that this is the first detailed XPS line shape analysis of a monolayer of an organic molecule, significantly larger than benzene, on a well-defined substrate.

Acknowledgment. We gratefully acknowledge the experimental support provided during the beam time by the BESSY staff, especially by Drs. C. Jung and D. Bachelor, and by H. Marchetto, Fritz-Haber-Institut Berlin. This work was funded by the German Bundesminister für Bildung und Forschung under Contract 05 KS WWA/5 and by the Deutsche Forschungsgemeinschaft through Projects Um 6/8-1,2. One of us (E.U.) acknowledges support by the Fonds der Chemischen Industrie.

References and Notes

(1) Lei, T.; Lee, J.; Zei, M. S.; Ertl, G. *J. Elektroanal. Chem.* **2003**, *41*−*48* 554.
(2) Koch, E. E. *Phys. Scripta* **1987**, *T17*, 120.
(3) Salaneck, W. R. *Crc. Cr. Rev. Sol. State.* **1985**, *12*, 267.
(4) Hirose, Y.; Kahn, A.; Aristov, V.; Soukiassian, P.; Bulovic, V.; Forrest, S. R. *Phys. Rev. B* **1996**, *54*, 13748.
(5) Tsiper, E. V.; Soos, Z. G.; Gao, W.; Kahn, A. *Chem. Phys. Lett.* **2002**, *360*, 47.
(6) Ishii, H.; Sugiyama, K.; Ito, E.; Seki, K. *Adv. Mater.* **1999**, *11*, 605.
(7) Ishii, H.; Sugiyama, K.; Ito, E.; Seki, K. *Adv. Mater*. **1999**, *11*, 972.
(8) Seki, K.; Hayashi, N.; Oji, H.; Ito, E.; Ouchi, Y.; Ishii, H. *Thin Solid Films* **2001**, *393*, 298−303.
(9) Umbach, E.; Glöckler, K.; Sokolowski, M. *Surf. Sci*. **1998**, *404*, 20.
(10) Fink, R.; Gador, D.; Stahl, U.; Zou, Y.; Umbach, E. *Phys. Rev. B* **1999**, *60*, 2818.
(11) Gador, D.; Zou, Y.; Buchberger, C.; Bertram, M.; Fink, R.; Umbach, E. *J. Electron Spectrosc.* **1999**, *101*−*103*, 523.
(12) Soukopp, A.; Glöckler, K.; Kraft, P.; Schmitt, S.; Sokolowski, M.; Umbach, E.; Mena-Osteritz, E.; Bäuerle, P.; Hädicke, E. *Phys. Rev. B* **1998**, *58*, 13882.
(13) Tautz, F. S.; Eremtchenko, M.; Schäfer, J. A.; Sokolowski, M.; Shklover, V.; Glöckler, K.; Umbach, E. *Surf. Sci.* **2002**, *502*−*503*, 176.
(14) Glöckler, K.; Seidel, C.; Soukopp, A.; Sokolowski, M.; Umbach, E.; Böhringer, M.; Berndt, R.; Schneider, W.-D. *Surf. Sci*. **1998**, *405*, 1.
(15) Stahl, U.; Gador, D.; Soukopp, A.; Fink, R.; Umbach, E. *Surf. Sci.* **1998**, *414*, 423.
(16) Gador, D. Doctoral thesis, Universität Würzburg, 1999.
(17) Kilian, L. Doctoral thesis, Universität Würzburg, 2002.
(18) Kilian, L.; Schöll, A.; Zou, Y.; Fink, R.; Umbach, E. unpublished results.
(19) Shklover, V. Doctoral thesis, Universität Würzburg, 2002.
(20) Gador, D.; Buchberger, C.; Fink, R.; Umbach, E. *J. Electron Spectrosc.* **1998**, *96*, 11.
(21) Gador, D.; Fink, R.; Umbach, E. *Europhys. Lett.* **1998**, *41*, 231.
(22) Schöll, A.; Zou, Y.; Hübner, D.; Gador, D.; Kilian, L.; Jung, C.; Umbach, E. *Phys. Rev. Lett.* submitted.
(23) Carlson, T. A.; Dress, W. B.; Grimm, F. A.; Haggerty, J. S. *J. Electron Spectrosc*. **1977**, *10*, 147.
(24) Carlson, T. A. *Ann. Rev. Phys. Chem.* **1975**, *26*, 211.
(25) Spears, D. P.; Fischbeck, H. J.; Carlson, T. A. *J. Electron Spectrosc*. **1975**, *6*, 411.
(26) Gelius, U. *J. Electron Spectrosc*. **1974**, 5, 985.
(27) Umbach, E. *Surf. Sci*. **1982**, *117*, 482.
(28) Breitschafter, M. J.; Umbach, E.; Menzel, D. *Surf. Sci*. **1981**, *109*, 493. Umbach, E.; Kulkarni, S.; Feulner, P.; Menzel, D. *Surf. Sci*. **1979**, *88*, 65.
(29) Nilsson, A.; Tillborg, H.; Martensson, N. *Phys. Rev. Lett.* **1991**, *67*, 1015.
(30) Wurth, W.;Schneider, C.; Treichler, R.; Umbach, E.; Menzel, D. *Phys. Rev. B* **1987**, *35*, 7741.
(31) Nilsson, A.; Stenborg, A.; Tillborg, H.; Gunnelin, K.; Martensson, N. *Phys. Rev. B* **1993**, *47*, 13590. Tillborg, H.; Nilsson, A.; Martensson, N. *J. Electron Spectrosc.* **1993**, *62*, 73.
(32) Umbach, E.; Fuggle, J. C.; Menzel, D. *J. Electron Spectrosc*. **1977**, *10*, 15. Fuggle, J. C.; Umbach, E.; Feulner, P.; Menzel, D. *Surf. Sci*. **1977**, *64*, 69.
(33) Freund, H. J.; Bigelow, R. W. *Phys. Scripta* **1987**, *T17*, 50.
(34) Bigelow, R. W.; Law, K. Y.; Pan, D. H. K.; Freund, H. J. *J. Electron Spectrosc.* **1988**, *46*, 1.
(35) Yang, L.; Agren, H. *Phys. Rev. B* **1996**, *54*, 13649.
(36) Jung, M.; Bason, U.; Porwol, T.; Freund, H.-J.; Umbach, E. in preparation.
(37) Martensson, N.; Baltzer, P.; Bruhwiler, P. A.; Forsell, J. O.; Nilsson, A.; Stenborg, A.; et al. *J. Electron Spectrosc*. **1994**, *70*, 117.
(38) Schöll, A.; Zou, Y.; Schmidt, T.; Fink, R.; Umbach, E. *J. Electron Spectrosc.* **2003**, *129*, 1.
(39) Schöll, A.; Zou, Y.; Schmidt, T.; Fink, R.; Umbach, E. *J. Electron Spectrosc.* in preparation.
(40) Schöll, A.; Kilian, L.; Zou, Y.; Schmidt, T.; Fink, R.; Umbach, E. in preparation.
(41) Hübner, D.; Kilian, L.; Schöll, A.; Fink, R.; Umbach, E. in preparation.
(42) Fuggle, J. C.; Menzel, D. *Vakuum-Technik* **1978**, *27*, 130.
(43) Hermann, K.; Bagus, P. S.; Brundle, C. R.; Menzel, D. *Phys. Rev. B* **1981**, *24*, 7025.
(44) Brundle, C. R.; Bagus, P. S.; Menzel, D.; Hermann, K. *Phys. Rev. B* **1981**, *24*, 7041.
(45) Bagus, P. S.; Hermann, K. *Surf. Sci.* **1979**, *89*, 588.
(46) Hermann, K.; Bagus, P. S. *Phys. Rev. B* **1977**, *16*, 4195.
(47) Bagus, P. S.; Hermann, K.; Seel, M. *J. Vac. Sci. Technol.* **1981**, *18*, 435.
(48) Messmer, R. P.; Lamson, S. H.; Salahub, D. R. *Phys. Rev. B* **1982**, *25*, 3576.
(49) Schönhammer, K.; Gunnarsson, O. *Sol. State Comm.* **1977**, *23*, 691.
(50) Gunnarsson, O.; Schönhammer, K. *Phys. Rev. Lett.* **1978**, *41*, 1608.
(51) Schönhammer, K.; Gunnarsson, O. *Surf. Sci*. **1979**, *89*, 575.